

Article

Study on the Performance of Cellulose Triacetate Hollow Fiber Mixed Matrix Membrane Incorporated with Amine-Functionalized NH₂-MIL-125(Ti) for CO₂ and CH₄ Separation

Naveen Sunder ^{1,2}, Yeong-Yin Fong ^{1,2,*}, Mohamad Azmi Bustam ^{1,3}  and Woei-Jye Lau ⁴ ¹ Department of Chemical Engineering, Universiti Teknologi PETRONAS, Seri Iskandar 32610, Perak, Malaysia² CO₂ Research Center (CO₂RES), R&D Building, Universiti Teknologi PETRONAS, Seri Iskandar 32610, Perak, Malaysia³ Centre of Research in Ionic Liquids (CORIL), Universiti Teknologi PETRONAS, Seri Iskandar 32610, Perak, Malaysia⁴ Advanced Membrane Technology Research Centre (AMTEC), Faculty of Chemical and Energy Engineering, Universiti Teknologi Malaysia, Skudai 81310, Johor, Malaysia

* Correspondence: yinfong.yeong@utp.edu.my

Abstract: The increase in the global population has caused an increment in energy demand, and therefore, energy production has to be maximized through various means including the burning of natural gas. However, the purification of natural gas has caused CO₂ levels to increase. Hollow fiber membranes offer advantages over other carbon capture technologies mainly due to their large surface-to-volume ratio, smaller footprint, and higher energy efficiency. In this work, hollow fiber mixed matrix membranes (HFMMMs) were fabricated by utilizing cellulose triacetate (CTA) as the polymer and amine-functionalized metal-organic framework (NH₂-MIL-125(Ti)) as the filler for CO₂ and CH₄ gas permeation. CTA and NH₂-MIL-125(Ti) are known for exhibiting a high affinity towards CO₂. In addition, the utilization of these components as membrane materials for CO₂ and CH₄ gas permeation is hardly found in the literature. In this work, NH₂-MIL-125(Ti)/CTA HFMMMs were spun by varying the air gap ranging from 1 cm to 7 cm. The filler dispersion, crystallinity, and functional groups of the fabricated HFMMMs were examined using EDX mapping, SEM, XRD, and FTIR. From the gas permeation testing, it was found that the NH₂-MIL-125(Ti)/CTA HFMMM spun at an air gap of 1 cm demonstrated a CO₂/CH₄ ideal gas selectivity of 6.87 and a CO₂ permeability of 26.46 GPU.

Keywords: metal-organic frameworks (MOFs); NH₂-MIL-125(Ti); cellulose triacetate; hollow fiber mixed matrix membranes; CO₂/CH₄ separation



Citation: Sunder, N.; Fong, Y.-Y.; Bustam, M.A.; Lau, W.-J. Study on the Performance of Cellulose Triacetate Hollow Fiber Mixed Matrix Membrane Incorporated with Amine-Functionalized NH₂-MIL-125(Ti) for CO₂ and CH₄ Separation. *Separations* **2023**, *10*, 41. <https://doi.org/10.3390/separations10010041>

Academic Editor: Zhun Ma

Received: 5 December 2022

Revised: 15 December 2022

Accepted: 19 December 2022

Published: 9 January 2023



Copyright: © 2023 by the authors. Licensee MDPI, Basel, Switzerland. This article is an open access article distributed under the terms and conditions of the Creative Commons Attribution (CC BY) license (<https://creativecommons.org/licenses/by/4.0/>).

1. Introduction

With the global energy demand expected to increase by 3% in 2022 after its decline in 2020 due to the COVID-19 pandemic, the use of fossil fuels still maintains as the main supplying source for energy [1,2]. Consequently, this leads to a rise in global CO₂ emissions to 38.0 Gt CO₂, with fossil fuels contributing a 0.6% increase in CO₂ emissions [3]. Although the purification of natural gas contributes to the rise in CO₂ emissions, it is still considered as the cleanest form of energy among fossil fuels [4]. With nearly 37 Tcf of sour natural gas, Malaysia's gas fields remain undeveloped due to the presence of a high content of acidic gas which mainly consists of CO₂ [5]. For example, in Sarawak, the gas fields show CO₂ contents of up to 87% [6]. Moreover, gas pipeline specifications only allow the presence of small quantities of CO₂ because the existence of a high amount of acidic gases will create problems for gas production financially and operationally [7]. Therefore, the removal of CO₂ from natural gas is mandatory.

Since the past decade, several technologies have been reported and implemented in gas processing industries to reduce the acid gas composition in sour natural gas. These

include cryogenic distillation, amine adsorption, pressure swing adsorber, and temperature swing adsorber. However, these technologies suffer certain drawbacks such as high energy consumption, high carbon footprint production, high capital, and regeneration cost [8–11]. Thus, membranes for gas separation have gained popularity due to their advantages over the aforementioned technologies.

Membranes act as a semipermeable barrier that only allows certain molecules to pass through while restricting the penetration of other particles. Membrane technologies have been utilized in various industrial applications such as wastewater treatment and gas separation [12]. Furthermore, membrane technologies offer several advantages over other separation technologies such as ease of operability, low footprint, cost-effectiveness, and low energy consumption [13]. With such advantages, membrane technologies have managed to attract considerable attention in recent years. However, membranes face challenges that include fouling, structural integrity, and most importantly, the tradeoff between permeability and selectivity [14]. Despite that, membranes are able to be fine-tuned by optimizing the materials used and the configurations applied to minimize or overcome the limitations faced by conventional flat-sheet membranes.

There are several types of materials that can be used for natural gas sweetening, most commonly polymeric, inorganic, metal-organic frameworks (MOFs), and mixed matrix membranes (MMMs) [15]. The most widely commercialized type of membrane is polymeric membranes, which have constantly undergone improvements to increase their CO₂ permeability and selectivity. However, polymeric membranes have a key limitation, which is the tradeoff between permeability and selectivity as illustrated by the Robeson's upper limit bound [16,17]. Polymeric membranes can be made from materials such as cellulose acetate, polysulfone, polyimide, and poly(ethyleneimine) [16]. Notably, cellulose acetate (CA) is a popular type of polymeric membrane used in various industries [18]. CA exhibited a CO₂ permeability of 6.0 Barrer and a CO₂/CH₄ selectivity of 29 at a temperature and pressure of 35 °C and 27 kPa, respectively [19]. On the other hand, cellulose triacetate (CTA) demonstrated a higher affinity towards CO₂ compared to CH₄, which may result in greater gas separation capabilities despite being nearly chemically identical to CA but with a higher degree of hydrophobicity [20]. Furthermore, CTA is preferable compared to other polymers due to its low cost, ease of availability, and good mechanical and chemical stability [21]. It is noteworthy that the higher degree of acetylation of CTA exhibits higher CO₂ permeability with lower CO₂/CH₄ selectivity [22].

Metal-organic frameworks (MOFs) are an innovative type of unique hybrid between organic and inorganic materials with an exceptionally high surface area and flexibility in pore size, shape, and structure [23–30]. The drawback of using a pure MOF film membrane for gas separation is the weak membrane–substrate bonding due to low adhesion forces which cause cracks and defects the formation on the membrane during drying or thermal activation [31,32]. To counteract the disadvantages of the polymeric and MOF-type membranes, MMMs are utilized as they provide the benefits of both organic and inorganic materials, with the polymer acting as a continuous phase and the filler serving as the dispersed phase. The frequently used fillers for MMMs fabrication include MOFs [29,33], zeolites [34], carbon [35], and metal oxides [36]. MOFs such as ZIF-8 [37,38], NH₂-UiO-66(Zr) [39,40], NH₂-MOF-199 [41], and NH₂-MIL-125(Ti) [42] are among the most commonly researched fillers for the fabrication of MMMs in recent studies with high gas separation potential. The material selection for MOFs is crucial based on their purpose, pore size, and shape in order to ensure the desired separation performance [43]. In addition, amine-functionalized NH₂-MIL-125(Ti) that contains octa-nuclear Ti-clusters can form a relatively cubic tetragonal structure arranged by 2-amino-1,4-benzenedicarboxylate ligands. Amine functionalization of the MOF allows facilitated diffusion to occur between the CO₂ gas molecule and the NH₂ carrier through reversible chemical reactions, therefore allowing CO₂ to have a higher capture rate [44].

In a recent study reported by Mehmood et al. [45], the incorporation of a 0.4 wt% gamma-cyclodextrin (γ -CD) MOF into CA polymer was performed to fabricate a CA/ γ -

CD MMM with a CO₂/CH₄ selectivity of 38.49 with a CO₂ permeability of 17 barrer. By comparison, pure CA obtained a CO₂/CH₄ selectivity of 1.9 with a CO₂ permeability of 19 barrer. They concluded that the glassy nature of CA results in a decrease in CO₂ permeability but an increase in CO₂/CH₄ selectivity when CA is used for MMM fabrication. Moreover, Saneepur et al. [46] fabricated novel ion-exchanged zeolite (Co(II)-NaY)/CA MMMs at various loadings for CO₂/N₂ separation. Their research found that 15 wt% of Co(II)-NaY was an optimal loading in the CA matrix, which demonstrated a 43.9% and 14.5% CO₂ gas permeation and CO₂/N₂ selectivity improvement, respectively, compared to the neat CA membrane, which resulted in a CO₂ permeability of 3.28 barrer and a CO₂/N₂ selectivity of 29.2.

On the other hand, substituting a flat sheet membrane configuration with the industrially preferred hollow fiber configuration provides various benefits. For example, an increase in surface area to volume ratio due to it being cylindrical, and thus an increase in the gas penetration through the membrane [47]. HFMMMs have the potential to increase the membrane performance further, provided that the materials selected are compatible to prevent particle agglomeration, which could potentially deteriorate the performance of the membrane [44].

In this work, NH₂-MIL-125(Ti) filler is incorporated into CTA polymer to form NH₂-MIL-125(Ti)/CTA HFMMMs which are fabricated using a dry-wet phase inversion method. Neat CTA HFMs are also fabricated and used as a benchmark for the overall gas permeation process. The permeation of CO₂ and CH₄ gas and the CO₂/CH₄ gas pair selectivity of the resultant membranes at a fixed pressure and temperature are assessed. In addition, characterization studies using energy-dispersive X-ray spectroscopy (EDX), scanning electron microscope (SEM), X-ray diffraction (XRD), and Fourier-transform infrared spectroscopy (FTIR), are conducted to analyze the filler dispersion, morphology, crystallinity, and functional groups of the resultant membranes.

2. Materials and Methods

2.1. Materials

Cellulose triacetate (CTA, $d = 1.3 \text{ g/cm}^3$, purity > 99.99%) and polydimethylsiloxane (PDMS, $d = 95 \text{ g/mL}^3$, purity > 99.99%) were acquired from ACROS Organics (Malaysia). Methanol (purity > 99.9%), N-methyl-2-pyrrolidone (NMP, purity > 99.8%), and n-hexane (purity > 99.99%) were obtained from Merck.

2.2. CTA HFM and NH₂-MIL-125(Ti)/CTA HFMMM Fabrication

The fabrication of CTA HFMs and NH₂-MIL-125(Ti)/CTA HFMMMs was conducted using a dry-wet phase inversion method. The NH₂-MIL-125 MOF filler was synthesized based on the method reported in our previous work [42]. A vacuum oven set at 60 °C was used to dry the CTA pellets overnight. CTA/NMP dope solution with a pre-determined critical concentration of 13 wt% was then prepared. The CTA pellets were added to the NMP solution and continuously stirred overnight until they completely dissolved. The NH₂-MIL-125(Ti)/CTA HFMMM with 1% filler loading was fabricated by firstly preparing a CTA/NMP solution and a NH₂-MIL-125(Ti)/NMP suspension which were separately stirred overnight. The suspension was then added periodically into the CTA/NMP solution, and the final dope solution was further stirred overnight.

The bore fluid, NMP/DI water (90%/10%) solution was then prepared and pumped at 0.33 mL/min during the spinning process, while 3.5 rpm was used to extrude the CTA/NMP solution from the spinneret under N₂ atmosphere. The extruded fibers were passed through the coagulant bath at 25 °C and collected using a take-up drum with its speed adjusted to free-fall. A range between 1 cm and 7 cm was used as the air gap distance. Table 1 lists the spinning parameters for the CTA HFMs and the NH₂-MIL-125(Ti)/CTA HFMMMs spun in this study.

Table 1. Parameters for the spinning of CTA HFM and NH₂-MIL-125(Ti)/CTA HFMMM.

Parameters	Conditions
Dope Solutions	CTA/NMP NH ₂ -MIL-125(Ti)/CTA/NMP
CTA (wt%)	13
Bore Fluid (NMP/Water, wt%)	90/10
Spinneret Dimensions (OD/ID, mm)	0.8/0.4
Dope Flow Rate (rpm)	3.5
Bore Flow Rate (mL/min)	0.33
Coagulant Temperature (°C)	25
Air Gap Distance (cm)	1, 3, 5 and 7

2.3. Solvent Exchange

The NMP solvent presence in the spun fibers was removed by solvent exchange using plain water, methanol, and n-hexane [48–50]. Firstly, water was used to soak the fibers for three days, with fresh water supplied between four hours and eight hours. Next, fibers were dipped into the methanol solvent for 30 min, 3 times, under mild stirring. This step was repeated by changing the methanol with n-hexane. Finally, the fibers were dried under ambient conditions for three days before use.

2.4. Post-Treatment

Post-treatment was conducted by coating the CTA HFMs and NH₂-MIL-125(Ti)/CTA HFMMMs with PDMS. PDMS coating has been found to seal certain non-selective defects and also enhance the permeation of gas over the coated membranes. The PDMS solution was prepared using 3 wt% PDMS in n-hexane under continuous stirring [51]. The fibers were immersed in the PDMS solution for 10 min under mild stirring. Next, the fibers were air-dried at room temperature for at least 48 h. After coating and drying, the fibers proceeded to gas permeation testing and characterization study.

2.5. Characterization

The morphology of the NH₂-MIL-125(Ti)/CTA HFMMMs was observed using a scanning electron microscope (SEM, Hitachi brand, model TM3030Plus). The fibers were split into smaller fibers after being submerged in liquid nitrogen. Then, the fibers were attached to a membrane holder and inserted inside the SEM machine. The SEM chamber was then vacuumed to avoid any discharge of electricity. Cross-sectional images of the membranes were then observed at 15 kV. Energy dispersive X-ray (EDX) was also used to examine the distribution of NH₂-MIL-125(Ti) in the hollow fiber membranes through elemental mapping. Next, X-ray diffraction (XRD, Panalytical, Model: Xpert3 Powder) was used to determine the membrane crystallinity. The XRD was operated at temperatures of 25 °C with an electron beam energy set at 45 kV and 40 mA under vacuum conditions. The X-ray beams were diffracted within the XRD to produce the peaks at varying 2θ range. For the membrane samples, the diffraction data was collected at a scan step size of 0.026 for 2θ ranged from 5° to 40°.

Fourier Transform Infrared spectroscopy (FTIR, Perkin Elmer, Model: Frontier 01) was used to identify the chemical bonds present in the molecular structure of the membranes based on the ATR method. The FTIR spectrum of the fibers was achieved between 550 cm⁻¹ and 4000 cm⁻¹ under the transmittance mode at room temperature.

2.6. CO₂ and CH₄ Gas Permeation Testing

A module containing three fibers was prepared. Epoxy resin was used to fully seal one end of the module and partially seal the other end of the module as the permeate side. The epoxy was air-dried at room temperature for 48 h. Next, the module, after drying, was placed in a gas permeation housing cell and tightly sealed. The temperature and flowrate of the feed gas were set at 25 °C and 200 mL/min, respectively, and the gas was

fed into the module’s shell side. A bubble flow meter and stopwatch were used to record the time taken for the bubble to reach a specific point. The time is used to measure the volumetric flowrate of permeate gas followed by the calculation of the CO₂ permeance using Equation (1) as follows [52]:

$$\frac{P_{CO_2}}{L} = \frac{Q}{A\Delta P} = \frac{Q}{n\pi DL_m\Delta P} \tag{1}$$

where n , L_m (cm), Q (cm³/min), ΔP (cmHg), and D (cm) are the number of fibers, the effective length of fibers in each module, permeate flow rate, pressure drop, and outer diameter, respectively. P_{CO_2} is the permeance of CO₂ of the fiber measured in GPU (1 GPU = 1 × 10⁻⁶ cm³ (STP)/cm².s.cmHg). The CO₂/CH₄ ideal selectivity was calculated using Equation (2) [52]:

$$\alpha_{CO_2/CH_4} = \frac{P_{CO_2}}{P_{CH_4}} \tag{2}$$

Figure 1 shows the gas permeation testing set up used in the current work [53].

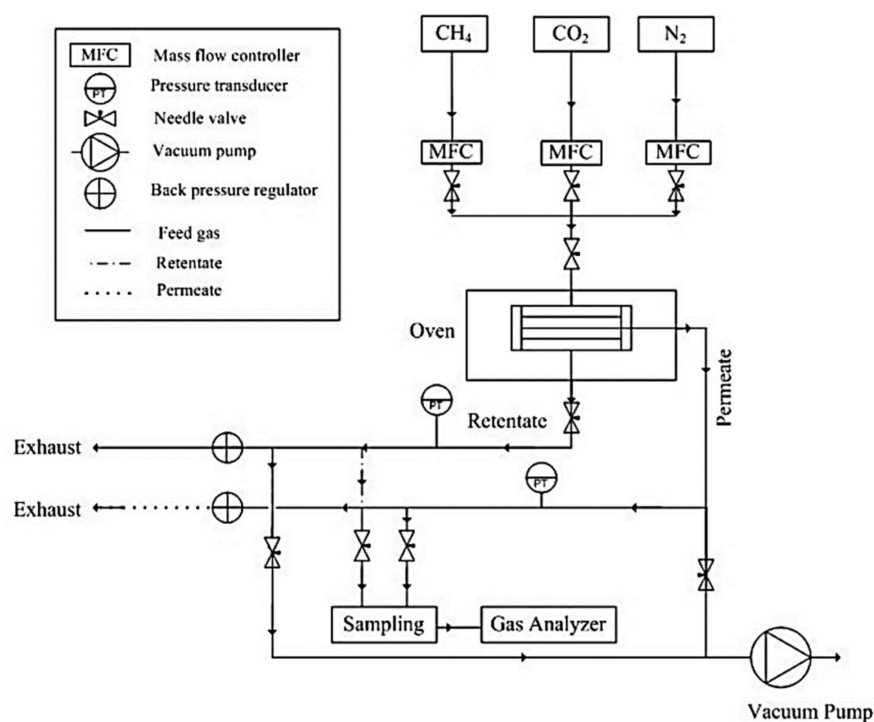


Figure 1. Equipment design for the in-house gas permeation test system used for the experiment [53].

3. Results and Discussion

3.1. Fabricated Membrane Characterization

Several characterizations were performed which included EDX, SEM, XRD, and FTIR to analyze the NH₂-MIL-125(Ti) filler dispersion, morphology, crystallinity, and functional groups of the resultant membranes.

3.1.1. Energy Dispersive X-ray (EDX) and Scanning Electron Microscope (SEM)

Figure 2 shows the dispersion of NH₂-MIL-125(Ti) fillers in the HFMMMs at varying air gaps using EDX mapping. The blue points shown in the EDX mapping represent the dispersed Ti elements on the surface of the HFMMMs. From Figure 2, it can be seen that the Ti elements were homogeneously dispersed with the absence of any agglomeration at all air gaps, possibly due to the use of a low NH₂-MIL-125(Ti) loading percentage (1 wt%) in the HFMMMs.

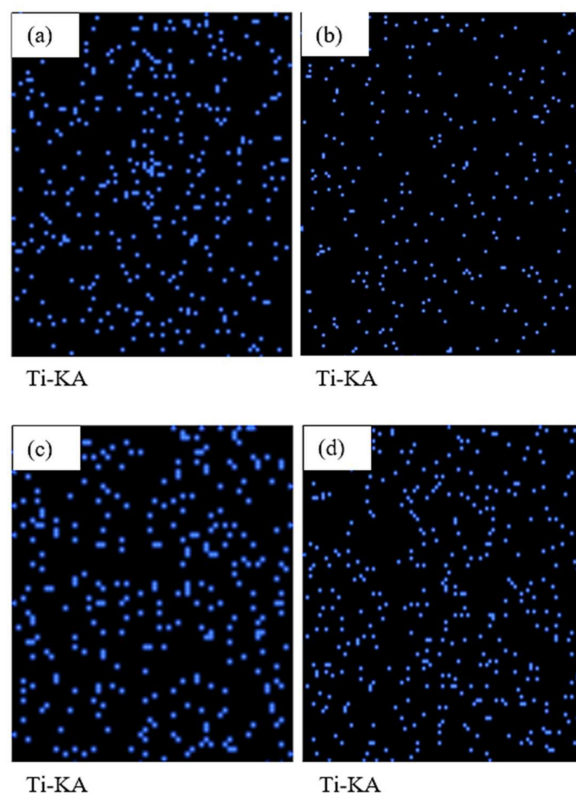


Figure 2. $\text{NH}_2\text{-MIL-125(Ti)/CTA}$ HFMMMs spun at various air gap distances of (a) 1 cm, (b) 3 cm, (c) 5 cm, and (d) 7 cm.

Figure 3 shows the cross-sectional SEM images of the $\text{NH}_2\text{-MIL-125(Ti)/CTA}$ HFMMMs spun at air gap distances ranging from 1 cm to 7 cm. As shown in Figure 3, macrovoids are present in all membranes. The presence of the macrovoids could possibly be due to the non-solvent intrusion during die swell and also from the Marangoni effect [21,54], which could affect the gas permeation performance of the membranes.

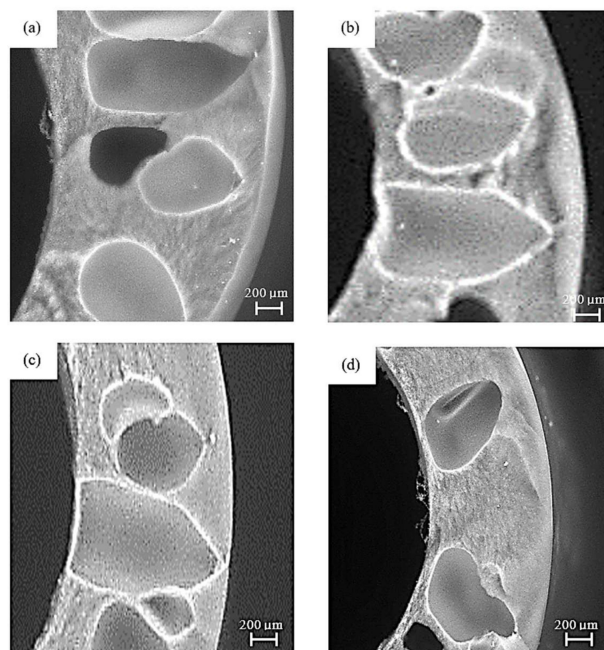


Figure 3. SEM cross-sectional images of $\text{NH}_2\text{-MIL-125(Ti)/CTA}$ HFMMM spun at different air gap distances of (a) 1 cm, (b) 3 cm, (c) 5 cm, and (d) 7 cm.

3.1.2. X-ray Diffraction (XRD) of Resultant Membranes

XRD was utilized to examine the crystalline structure of the NH₂-MIL-125(Ti)/CTA HFMMM. The neat CTA HFM and NH₂-MIL-125(Ti)/CTA HFMMM XRD spectra are observed in Figure 4. From the analysis, broad amorphous peaks are found at 8° and 17°, which suggests the presence of the cellulose triacetate polymer structure [55]. However, with the incorporation of the filler into the CTA polymer, it can be observed that the peaks are slightly more prominent in the HFMMM. No other significant peak was observed for the HFMMM possibly due to the incorporation of a relatively low loading of the NH₂-MIL-125(Ti) filler.

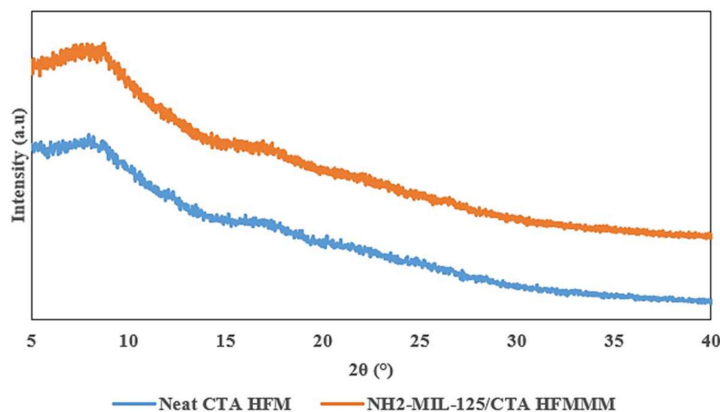


Figure 4. XRD pattern of CTA HFM and NH₂-MIL-125(Ti)/CTA HFMMM.

3.1.3. Fourier-Transformed Infrared (FTIR) Spectra of Resultant Membranes

FTIR was used to identify the interactions and chemical functionalities between CTA polymer and NH₂-MIL-125(Ti) filler. The FTIR spectra of the CTA HFMs and NH₂-MIL-125(Ti)/CTA HFMMMs for the band vibrations between 550 cm⁻¹ and 4000 cm⁻¹ are shown in Figure 5. The peaks found at 3530 cm⁻¹, 2956 cm⁻¹, and 1752 cm⁻¹ for CTA HFM represent the O-H stretch bond, the C-H stretch bond, and the C=O stretch band, respectively [56]. The acetyl group was observed by the C-O stretch at 1220 cm⁻¹, while the C-O-C stretch which represents the cellulose backbone was observed at 1040 cm⁻¹ [55]. Similar CTA spectra were also reported elsewhere [57]. From the spectra analysis, both fibers showed ester characteristic adsorption bands based on the C=O stretching at 1752 cm⁻¹ and the CH₃ symmetrical deformation at 1371 cm⁻¹ [58]. Moreover, with the addition of the NH₂-MIL-125(Ti) filler in the HFMMMs, an NH₂-group was identified in between the minor broad peaks of 3530 cm⁻¹ and 3350 cm⁻¹, despite the low loading percentage of 1 wt% [59–61].

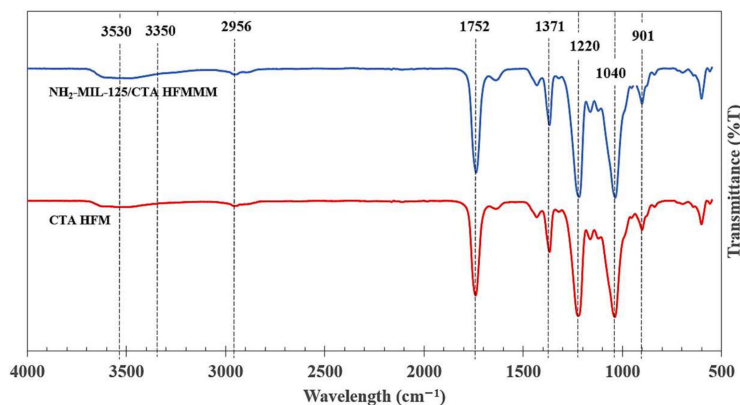


Figure 5. FTIR Spectra of CTA HFMs and NH₂-MIL-125(Ti)/CTA HFMMMs.

3.2. CO₂ and CH₄ Gas Permeation Study

In this current study, CO₂ and CH₄ gas permeation testing was conducted for CTA HFMs and NH₂-MIL-125(Ti)/CTA HFMMMs at ambient temperature and feed pressure of 5 bar gauge. Figures 6–8 show the CO₂ gas permeability, CH₄ gas permeability, and CO₂/CH₄ gas pair selectivity of all fabricated fibers, respectively.

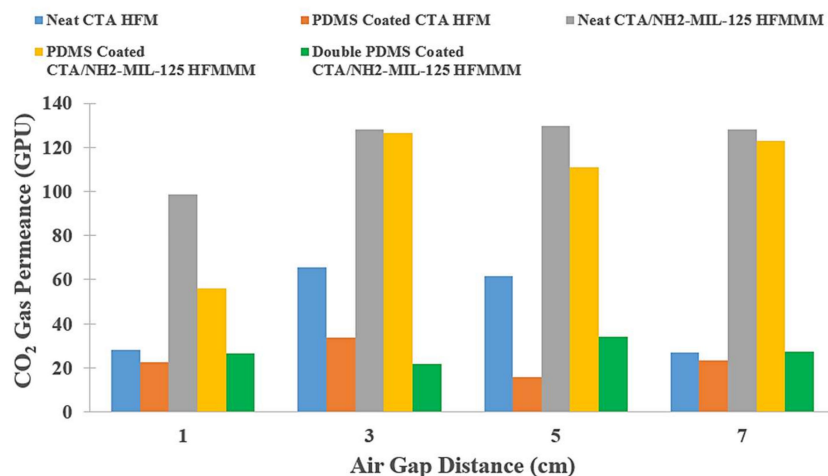


Figure 6. CO₂ gas permeance for the fabricated fibers at various air gap distances.

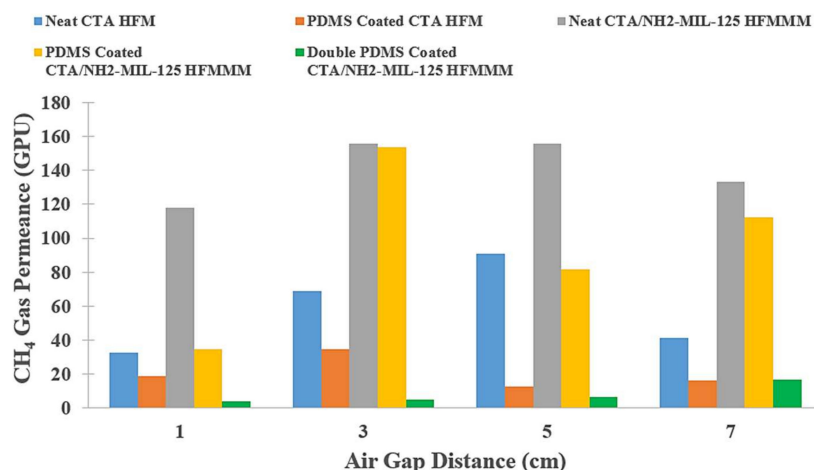


Figure 7. CH₄ gas permeance for the fabricated fibers at various air gap distances.

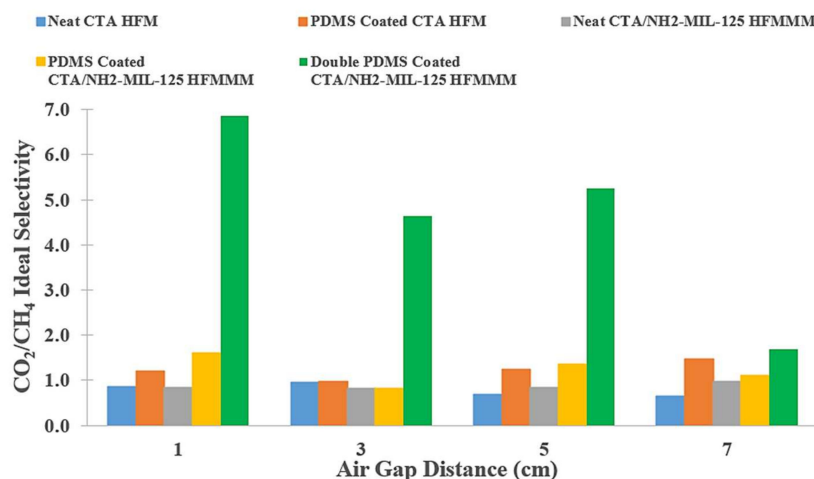


Figure 8. CO₂/CH₄ gas pair ideal selectivity for the fabricated fibers at various air gap distances.

The fabricated neat CTA HFMs spun at 1 cm to 3 cm showed an increase in CO₂ permeability followed by a gradual decrease in CO₂ permeability for the HFM spun at an air gap of 7 cm. Meanwhile, CH₄ permeability showed an increasing trend for the fibers spun at an air gap of 1 cm to 5 cm and then decreased for the fiber spun at 7 cm. Neat CTA HFMs spun at a 3 cm air gap demonstrated the highest CO₂ permeability at 65.68 GPU while CTA HFMs spun at a 5 cm air gap exhibited the highest CH₄ permeability of 90.69 GPU among CTA HFMs. However, neat CTA HFMs demonstrated low CO₂/CH₄ selectivity, possibly due to various surface defects. Therefore, PDMS coating which has been proven to reduce surface defects [51,62] was applied to the neat fibers to improve their gas permeation performance. Generally, PDMS-coated CTA HFMs showed a noticeable increment in CO₂/CH₄ selectivity with a significant drop in CO₂ and CH₄ permeability, especially for fibers spun at 3 and 5 cm air gaps, with a decrease in CO₂ permeability up to 95% and 295%, respectively. PDMS coated CTA HFMs spun at a 7 cm air gap revealed the highest increase in CO₂/CH₄ gas pair selectivity, from 0.65 to 1.47, with an improvement of 126%. Despite that, PDMS coated CTA HFM spun at a 3-cm air gap showed a very marginal improvement of CO₂/CH₄ selectivity, besides demonstrating a 95% and 50% decrease in CO₂ and CH₄ permeability, respectively.

On the other hand, neat NH₂-MIL-125(Ti)/CTA HFMMMs exhibited an improvement in gas permeation performance over the neat CTA HFMs due to the presence of an amine group, which resulted in the facilitated transport of CO₂ over the membrane. The increment of CO₂ permeability of up to 380% and CH₄ permeability of up to 264% with a slight improvement in CO₂/CH₄ gas pair selectivity was found for the HFMMM. The increase in CO₂ permeability may be attributed to the formation of defects and macrovoids found on the HFMMMs as seen in the SEM images in Figure 3. The CO₂ permeability increased initially as the air gap increased after 1 cm and then maintained a similar gas permeance of about 128 GPU from an air gap of 3 cm to 7 cm. Nevertheless, the high CO₂ and CH₄ gas permeability obtained could be due to the presence of defects and macrovoids on the HFMMM as observed in Figure 3 [21,44,63]. After the PDMS coating was applied to the resultant HFMMMs, a decrease in CO₂ permeability of 43% was observed for the HFMMM spun at an air gap of 1 cm, while the other HFMMMs spun at an air gap of 3 cm to 7 cm showed only a minor decrease in CO₂ permeability. Whereas, for the CH₄ permeability, a significant drop of 71% and 48% was observed for the fibers spun at an air gap of 1 cm and 5 cm, respectively. It can be observed that the HFMMM spun at an air gap of 3 cm showed lower performance compared to neat CTA HFMs, possibly due to the incorporation of the filler, which caused the stressing and widening of the macrovoids present on the membrane [64]. Subsequently, for the PDMS-coated HFMMM spun at an air gap of 1 cm, a noticeable tradeoff was observed, whereby the decrease in CO₂ and CH₄ gas permeability led to a slight increase in CO₂/CH₄ selectivity from 0.84 to 1.61. The improvements were 92% and 34% compared to the neat HFMMM and PDMS-coated HFM, respectively. An almost similar result trend was obtained for the PDMS-coated HFMMM spun at a 5 cm air gap. However, PDMS-coated HFMMMs spun at an air gap of 3 cm and 7 cm showed poorer results in terms of CO₂/CH₄ selectivity. This is likely due to the significant surface defects found on the fibers.

Moving on, a second layer of PDMS was applied to the NH₂-MIL-125(Ti)/CTA HFMMM to further seal any possible non-selective defects. From the CO₂/CH₄ selectivity results obtained (as shown in Figure 8), the HFMMMs coated with double PDMS layers performed better than the other membranes spun at all air gaps. HFMMM spun at an air gap of 1 cm showed the highest performance with a CO₂/CH₄ selectivity of 6.87, a CO₂ permeance of 26.46 GPU, and a CH₄ permeability of 3.85 GPU. Among the tested HFMMMs coated with double PDMS coating layers, a fluctuating CO₂/CH₄ gas pair selectivity was obtained as the air gap increased, with the lowest CO₂/CH₄ selectivity of 1.68 obtained for the fiber spun at an air gap of 7 cm. The low performance of the fiber at the highest air gap (7 cm) could possibly be due to instability caused by the overstretching of the polymer chain leading to elongation and gravitational stress. This may further increase defects

and macrovoids on the selective dense skin of the fiber, which was unable to be further improved by applying multiple PDMS coating layers [21,44,65].

In summary, HFMMMs coated with double PDMS layers showed a substantial boost in CO₂/CH₄ selectivity performance, especially for fibers spun at an air gap from 1 cm to 5 cm, but this led to a decrease in CO₂ and CH₄ permeability. A comparison between the CO₂/CH₄ gas permeability results of the current work with those results reported in the literature are presented in Table 2. Based on Table 2, the NH₂-MIL-125/CTA HFMMMs fabricated at an air gap distance of 1 cm performed better than the NH₂-MIL-53(Al)/CA HFMMM in terms of CO₂ permeance but with a lower CO₂/CH₄ selectivity, while against the NH₂-MIL-125(Ti)/PVDF HFMMM, it showed a greater CO₂/CH₄ selectivity and lower CO₂ permeance. Therefore, by comparison, the NH₂-MIL-125/CTA HFMMM prepared in this work show a reasonable gas separation performance with potential for improvement through optimization of the spinning parameters or filler loading.

Table 2. Comparison of CO₂/CH₄ gas permeability results of CTA HFM and NH₂-MIL-125(Ti)/CTA HFMMM in the current work with those results reported in the literature.

Membrane	Filler Loading (%)	Configuration	Air Gap Distance (cm)	Post Treatment	CO ₂ Permeance	CO ₂ /CH ₄ Ideal Selectivity	Ref
CTA	-	Hollow fiber	1	PDMS coating	22.49 GPU	1.20	This work
NH ₂ -MIL-125(Ti)/CTA	1	Hollow fiber	1	PDMS coating	26.46 GPU	6.87	This work
NH ₂ -MIL-53(Al)/CA	15	Hollow fiber	5	-	14.30 GPU	9.10	[66]
NH ₂ -MIL-125(Ti)/PVDF	1	Hollow fiber	15	-	350 GPU	4.00	[67]

4. Conclusions

In this study, NH₂-MIL-125(Ti)/CTA HFMMMs were successfully spun at different air gaps ranging from 1 to 7 cm. EDX mapping analysis showed that filler dispersion in the HFMMM was homogeneous with no indication of agglomeration, possibly due to the use of a low loading percentage of filler. SEM cross-sectional images of the fabricated fibers showed the presence of macrovoids in all spun fibers. The amorphous broad peaks were shown in the XRD result for CTA HFMs but with the incorporation of the filler in the HFMMM, an amorphous phase was still observed mainly due to the low loading of the filler. FTIR spectra revealed a broad peak between 3530 cm⁻¹ and 3350 cm⁻¹ for HFMMM compared to the spectrum obtained for CTA due to the incorporation of the NH₂-MIL-125(Ti) filler in CTA.

For the PDMS-coated CTA HFM, the best-performing fiber was found at a 7 cm air gap with a CO₂ permeability of 23.42 GPU and a CO₂/CH₄ selectivity of 1.47, which achieved a 126% improvement over the uncoated CTA HFMs. On the other hand, the HFMMM spun at a 1 cm air gap and coated with a double layer of PDMS showed a CO₂/CH₄ selectivity of 6.87 and a CO₂ permeance of 26.46 GPU. For future improvement, different loadings of fillers can be investigated to determine the optimum amount of filler required. Moreover, other spinning parameters such as the take-up speed and dope flowrate can be manipulated to find the optimum conditions for the enhancement of gas separation performance.

Author Contributions: Conceptualization, Y.-Y.F., M.A.B.; validation, Y.-Y.F.; formal analysis, N.S.; investigation, W.-J.L., N.S.; resources, M.A.B., Y.-Y.F.; data curation, N.S.; writing—original draft preparation, N.S.; writing—review and editing, W.-J.L., Y.-Y.F.; visualization, W.-J.L., N.S.; supervision, M.A.B., Y.-Y.F.; project administration, Y.-Y.F.; funding acquisition, Y.-Y.F. All authors have read and agreed to the published version of the manuscript.

Funding: This research was funded by Universiti Teknologi PETRONAS under the Joint Research Grant, cost center 015MDO-079 and the YUTP research grant, cost center 015LCO-099.

Institutional Review Board Statement: Not applicable.

Informed Consent Statement: Not applicable.

Data Availability Statement: Not applicable.

Acknowledgments: The financial and technical support provided by Universiti Teknologi PETRONAS under the Joint Research Grant (JRP, Cost Center: 015MD0-079), the Yayasan Universiti Teknologi PETRONAS (YUTP) Research Grant (Cost Center: 015LC0-099) and the CO₂ Research Centre (Cost Center: 015NEC-001), Universiti Teknologi PETRONAS are duly acknowledged.

Conflicts of Interest: The authors declare no conflict of interest.

References

1. International Agency Agency (IEA). Electricity Market Report—December 2020. Paris. 2020. Available online: <https://www.iea.org/reports/electricity-market-report-december-2020> (accessed on 11 October 2022).
2. Vega, F.; Cano, M.; Camino, S.; Fernández, L.M.G.; Portillo, E.; Navarrete, B. Solvents for Carbon Dioxide Capture. In *Carbon Dioxide Chemistry, Capture and Oil Recovery*; IntechOpen: London, UK, 2018. [CrossRef]
3. Olivier, J.G.J.; Peters, J.A.H.W. *Trends in Global CO₂ and Total Greenhouse Gas Emissions*; PBL Netherlands Environmental Assessment Agency: The Hague, The Netherlands, 2020; pp. 1–85.
4. Abu Bakar, W.A.W.; Ali, R. Natural Gas. In *Natural Gas*; Primož, P., Ed.; IntechOpen: Rijeka, 2010; p. Ch. 1.
5. Sukor, N.R.; Shamsuddin, A.H.; Mahlia, T.M.I.; Mat Isa, M.F. Techno-Economic Analysis of CO₂ Capture Technologies in Offshore Natural Gas Field: Implications to Carbon Capture and Storage in Malaysia. *Processes* **2020**, *8*, 350. [CrossRef]
6. Darman, N.H.; Harun, A.R. Technical Challenges and Solutions on Natural Gas Development in Malaysia. In Proceedings of the The petroleum Policy and Management (PPM) Project 4th Workshop of the China—Sichuan Basin Case Study, Beijing, China, 30 May–3 June 2006.
7. Hamad, F.; Qahtani, M.; Ameen, A.; Vaidya, M.; Duval, S.; Bahamdan, A.; Otaibi, F. Treatment of highly sour natural gas stream by hybrid membrane-amine process: Techno-economic study. *Sep. Purif. Technol.* **2020**, *237*, 116348. [CrossRef]
8. Riboldi, L.; Bolland, O. Overview on Pressure Swing Adsorption (PSA) as CO₂ Capture Technology: State-of-the-Art, Limits and Potentials. *Energy Procedia* **2017**, *114*, 2390–2400. [CrossRef]
9. Shang, J.; Hanif, A.; Li, G.; Xiao, G.; Liu, J.Z.; Xiao, P.; Webley, P.A. Separation of CO₂ and CH₄ by Pressure Swing Adsorption Using a Molecular Trapdoor Chabazite Adsorbent for Natural Gas Purification. *Ind. Eng. Chem. Res.* **2020**, *59*, 7857–7865. [CrossRef]
10. Grande, C.A. Advances in Pressure Swing Adsorption for Gas Separation. *ISRN Chem. Eng.* **2012**, *2012*, 982934. [CrossRef]
11. Mondino, G.; Grande, C.A.; Blom, R.; Nord, L.O. Moving bed temperature swing adsorption for CO₂ capture from a natural gas combined cycle power plant. *Int. J. Greenh. Gas Control.* **2019**, *85*, 58–70. [CrossRef]
12. McKeen, L.W. Markets and Applications for Films, Containers, and Membranes. In *Permeability Properties of Plastics and Elastomers*; William Andrew Publishing: Oxford, UK, 2012; pp. 59–75. [CrossRef]
13. Zhang, L.-Z. Heat and Mass Transfer in Hollow Fiber Membrane Bundles with Randomly Distributed Fibers. In *Conjugate Heat and Mass Transfer in Heat Mass Exchanger Ducts*; ResearchGate: Berlin, Germany, 2013; pp. 233–254.
14. Warsinger, D.M.; Chakraborty, S.; Tow, E.W.; Plumlee, M.H.; Bellona, C.; Loutatidou, S.; Karimi, L.; Mikelonis, A.M.; Achilli, A.; Ghassemi, A.; et al. A review of polymeric membranes and processes for potable water reuse. *Prog. Polym. Sci.* **2016**, *81*, 209–237. [CrossRef]
15. Wong, K.K.; Jawad, Z.A. A review and future prospect of polymer blend mixed matrix membrane for CO₂ separation. *J. Polym. Res.* **2019**, *26*, 289. [CrossRef]
16. Han, Y.; Ho, W.S.W. Recent advances in polymeric membranes for CO₂ capture. *Chin. J. Chem. Eng.* **2018**, *26*, 2238–2254. [CrossRef]
17. Robeson, L.M. The upper bound revisited. *J. Membr. Sci.* **2008**, *320*, 390–400. [CrossRef]
18. Scholes, C.A.; Stevens, G.W.; Kentish, S.E. Membrane gas separation applications in natural gas processing. *Fuel* **2012**, *96*, 15–28. [CrossRef]
19. Liu, C.; Wilson, S.T.; Kulprathipanja, S. Crosslinked Organic-Inorganic Hybrid Membranes and Their Use in Gas Separation. US 8,030,399 B2, 4 October 2011.
20. Chen, G.-J.; Lee, D.-J. Synthesis of asymmetrical cellulose acetate/cellulose triacetate forward osmosis membrane: Optimization. *J. Taiwan Inst. Chem. Eng.* **2019**, *96*, 299–304. [CrossRef]
21. Raza, A.; Askari, M.; Liang, C.Z.; Peng, N.; Farrukh, S.; Hussain, A.; Chung, T.-S. Advanced multiple-layer composite CTA/CDA hollow fiber membranes for CO₂ separations. *J. Membr. Sci.* **2021**, *625*, 119124. [CrossRef]
22. Puleo, A.C.; Paul, D.R.; Kelley, S.S. The effect of degree of acetylation on gas sorption and transport behavior in cellulose acetate. *J. Membr. Sci.* **1989**, *47*, 301–332. [CrossRef]
23. Ma, D.-Y.; Li, Z.; Xiao, J.-X.; Deng, R.; Lin, P.-F.; Chen, R.-Q.; Liang, Y.-Q.; Guo, H.-F.; Liu, B.; Liu, J.-Q. Hydrostable and Nitryl/Methyl-Functionalized Metal–Organic Framework for Drug Delivery and Highly Selective CO₂ Adsorption. *Inorg. Chem.* **2015**, *54*, 6719–6726. [CrossRef]

24. Liu, J.; Liu, G.; Gu, C.; Liu, W.; Xu, J.; Li, B.; Wang, W. Rational synthesis of a novel 3,3,5-c polyhedral metal–organic framework with high thermal stability and hydrogen storage capability. *J. Mater. Chem. A* **2016**, *4*, 11630–11634. [[CrossRef](#)]
25. Qin, N.; Pan, A.; Yuan, J.; Ke, F.; Wu, X.; Zhu, J.; Liu, J.; Zhu, J. One-Step Construction of a Hollow Au@Bimetal–Organic Framework Core–Shell Catalytic Nanoreactor for Selective Alcohol Oxidation Reaction. *ACS Appl. Mater. Interfaces* **2021**, *13*, 12463–12471. [[CrossRef](#)]
26. Qin, L.; Liang, F.; Li, Y.; Wu, J.; Guan, S.; Wu, M.; Xie, S.; Luo, M.; Ma, D. A 2D Porous Zinc–Organic Framework Platform for Loading of 5-Fluorouracil. *Inorganics* **2022**, *10*, 202. [[CrossRef](#)]
27. Qin, L.; Li, Y.; Liang, F.; Li, L.; Lan, Y.; Li, Z.; Lu, X.; Yang, M.; Ma, D. A microporous 2D cobalt-based MOF with pyridyl sites and open metal sites for selective adsorption of CO₂. *Microporous Mesoporous Mater.* **2022**, *341*, 112098. [[CrossRef](#)]
28. Feng, C.; Khulbe, K.C.; Matsuura, T.; Farnood, R.; Ismail, A.F. Recent Progress in Zeolite/Zeotype Membranes. *J. Membr. Sci. Res.* **2015**, *1*, 49–72.
29. Vinoba, M.; Bhagiyalakshmi, M.; Alqaheem, Y.; Alomair, A.A.; Pérez, A.; Rana, M.S. Recent progress of fillers in mixed matrix membranes for CO₂ separation: A review. *Sep. Purif. Technol.* **2017**, *188*, 431–450. [[CrossRef](#)]
30. Zheng, M.; Chen, J.; Zhang, L.; Cheng, Y.; Lu, C.; Liu, Y.; Singh, A.; Trivedi, M.; Kumar, A.; Liu, J. Metal organic frameworks as efficient adsorbents for drugs from wastewater. *Mater. Today Commun.* **2022**, *31*, 103514. [[CrossRef](#)]
31. Qian, Q.; Asinger, P.A.; Lee, M.J.; Han, G.; Mizrahi Rodriguez, K.; Lin, S.; Benedetti, F.M.; Wu, A.X.; Chi, W.S.; Smith, Z.P. MOF-Based Membranes for Gas Separations. *Chem. Rev.* **2020**, *120*, 8161–8266. [[CrossRef](#)] [[PubMed](#)]
32. Makarov, I.S.; Golova, L.K.; Bondarenko, G.N.; Anokhina, T.S.; Dmitrieva, E.S.; Levin, I.S.; Makhatova, V.E.; Galimova, N.Z.; Shambilova, G.K. Structure, Morphology, and Permeability of Cellulose Films. *Membranes* **2022**, *12*, 297. [[CrossRef](#)] [[PubMed](#)]
33. Vahabi, A.H.; Norouzi, F.; Sheibani, E.; Rahimi-Nasrabadi, M. Functionalized Zr–UiO-67 metal-organic frameworks: Structural landscape and application. *Coord. Chem. Rev.* **2021**, *445*, 214050. [[CrossRef](#)]
34. Castro-Munoz, R.; Fila, V. Progress on Incorporating Zeolites in Matrimid((R))5218 Mixed Matrix Membranes towards Gas Separation. *Membranes* **2018**, *8*, 30. [[CrossRef](#)]
35. Karousos, D.S.; Lei, L.; Lindbräthen, A.; Sapalidis, A.A.; Kouvelos, E.P.; He, X.; Favvas, E.P. Cellulose-based carbon hollow fiber membranes for high-pressure mixed gas separations of CO₂/CH₄ and CO₂/N₂. *Sep. Purif. Technol.* **2020**, *253*, 117473. [[CrossRef](#)]
36. Davood Abadi Farahani, M.H.; Chung, T.-S. Solvent resistant hollow fiber membranes comprising P84 polyimide and amine-functionalized carbon nanotubes with potential applications in pharmaceutical, food, and petrochemical industries. *Chem. Eng. J.* **2018**, *345*, 174–185. [[CrossRef](#)]
37. Sasikumar, B.; Bisht, S.; Arthanareeswaran, G.; Ismail, A.F.; Othman, M.H.D. Performance of polysulfone hollow fiber membranes encompassing ZIF-8, SiO₂/ZIF-8, and amine-modified SiO₂/ZIF-8 nanofillers for CO₂/CH₄ and CO₂/N₂ gas separation. *Sep. Purif. Technol.* **2021**, *264*, 118471. [[CrossRef](#)]
38. Gong, X.; Wang, Y.; Kuang, T. ZIF-8-Based Membranes for Carbon Dioxide Capture and Separation. *ACS Sustain. Chem. Eng.* **2017**, *5*, 11204–11214. [[CrossRef](#)]
39. Liu, B.; Li, D.; Yao, J.; Sun, H. Improved CO₂ separation performance and interfacial affinity of mixed matrix membrane by incorporating UiO-66-PEI@[bmim][Tf₂N] particles. *Sep. Purif. Technol.* **2020**, *239*, 116519. [[CrossRef](#)]
40. Jiang, Y.; Liu, C.; Caro, J.; Huang, A. A new UiO-66-NH₂ based mixed-matrix membranes with high CO₂/CH₄ separation performance. *Microporous Mesoporous Mater.* **2019**, *274*, 203–211. [[CrossRef](#)]
41. Shah Buddin, M.M.H.; Ahmad, A.L. A review on metal-organic frameworks as filler in mixed matrix membrane: Recent strategies to surpass upper bound for CO₂ separation. *J. CO₂ Util.* **2021**, *51*, 101616. [[CrossRef](#)]
42. Suhaimi, N.H.; Yeong, Y.F.; Jusoh, N.; Chew, T.L.; Bustam, M.A.; Suleman, S. Separation of CO₂ from CH₄ using mixed matrix membranes incorporated with amine functionalized MIL-125 (Ti) nanofiller. *Chem. Eng. Res. Des.* **2020**, *159*, 236–247. [[CrossRef](#)]
43. Wang, M.; Wang, Z.; Zhao, S.; Wang, J.; Wang, S. Recent advances on mixed matrix membranes for CO₂ separation. *Chin. J. Chem. Eng.* **2017**, *25*, 1581–1597. [[CrossRef](#)]
44. Li, G.; Kujawski, W.; Válek, R.; Koter, S. A review—The development of hollow fibre membranes for gas separation processes. *Int. J. Greenh. Gas Control.* **2021**, *104*, 103195. [[CrossRef](#)]
45. Mehmood, O.; Farrukh, S.; Hussain, A.; Younas, M.; Salahuddin, Z.; Pervaiz, E.; Ayoub, M. Investigation of cellulose acetate/gamma-cyclodextrin MOF based mixed matrix membranes for CO₂/CH₄ gas separation. *Greenh. Gases Sci. Technol.* **2021**, *11*, 313–330. [[CrossRef](#)]
46. Sanaeepur, H.; Kargari, A.; Nasernejad, B.; Ebadi Amooghin, A.; Omidkhan, M. A novel Co²⁺ exchanged zeolite Y/cellulose acetate mixed matrix membrane for CO₂/N₂ separation. *J. Taiwan Inst. Chem. Eng.* **2016**, *60*, 403–413. [[CrossRef](#)]
47. Chen, X.Y.; Kaliaguine, S.; Rodrigue, D. A Comparison between Several Commercial Polymer Hollow Fiber Membranes for Gas Separation. *J. Membr. Sep. Technol.* **2017**, *6*, 1–15. [[CrossRef](#)]
48. Bernardo, P.; Tasselli, F.; Chiappetta, G.; Clarizia, G. Effect of the Post-Spinning Solvent Exchange on the Performance of Asymmetric, Polyimide Hollow Fibers Prepared by Using a Triple-Orifice Spinneret. *Materials* **2019**, *12*, 3632. [[CrossRef](#)]
49. Isanejad, M.; Azizi, N.; Mohammadi, T. Pebax membrane for CO₂/CH₄ separation: Effects of various solvents on morphology and performance. *J. Appl. Polym. Sci.* **2017**, *134*, 44531. [[CrossRef](#)]
50. Zhu, H.; Jie, X.; Wang, L.; Kang, G.; Liu, D.; Cao, Y. Effect of MIL-53 on phase inversion and gas separation performance of mixed matrix hollow fiber membranes. *RSC Adv.* **2016**, *6*, 69124–69134. [[CrossRef](#)]

51. Hu, L.; Cheng, J.; Li, Y.; Liu, J.; Zhou, J.; Cen, K. Optimization of coating solution viscosity of hollow fiber-supported polydimethylsiloxane membrane for CO₂/H₂ separation. *J. Appl. Polym. Sci.* **2018**, *135*, 45765. [[CrossRef](#)]
52. Mubashir, M.; Yin fong, Y.; Leng, C.T.; Keong, L.K.; Jusoh, N. Study on the effect of process parameters on CO₂/CH₄ binary gas separation performance over NH₂-MIL-53(Al)/cellulose acetate hollow fiber mixed matrix membrane. *Polym. Test.* **2020**, *81*, 106223. [[CrossRef](#)]
53. Mubashir, M.; Yeong, Y.F.; Lau, K.K.; Chew, T.L. Effect of spinning conditions on the fabrication of cellulose acetate hollow fiber membrane for CO₂ separation from N₂ and CH₄. *Polym. Test.* **2019**, *73*, 1–11. [[CrossRef](#)]
54. Peng, N.; Chung, T.-S.; Wang, K.Y. Macrovoid evolution and critical factors to form macrovoid-free hollow fiber membranes. *J. Membr. Sci.* **2008**, *318*, 363–372. [[CrossRef](#)]
55. Shaikh, H.M.; Anis, A.; Poulouse, A.M.; Al-Zahrani, S.M.; Madhar, N.A.; Alhamidi, A.; Aldeligan, S.H.; Alsubaie, F.S. Synthesis and Characterization of Cellulose Triacetate Obtained from Date Palm (*Phoenix dactylifera* L.) Trunk Mesh-Derived Cellulose. *Molecules* **2022**, *27*, 1434. [[CrossRef](#)]
56. Raza, A.; Japip, S.; Liang, C.Z.; Farrukh, S.; Hussain, A.; Chung, T.S. Novel Cellulose Triacetate (CTA)/Cellulose Diacetate (CDA) Blend Membranes Enhanced by Amine Functionalized ZIF-8 for CO₂ Separation. *Polymers* **2021**, *13*, 2946. [[CrossRef](#)]
57. Jawaid, M.; Li, F.; Sun, M.; Cheng, Q.; Yang, B.; Kenawy, E.-R. Preparation and Characterization of Graphene Oxide/Cellulose Triacetate Forward Osmosis Membranes. *MATEC Web Conf.* **2016**, *67*, 1015. [[CrossRef](#)]
58. Cobo, F.N.; Faria-Tisher, P.C.S.; Duarte, J.L.; Carvalho, G.M. Preparation and characterization of microporous cellulose acetate films using breath figure method by spin coating technique. *Cellulose* **2017**, *24*, 4981–4995. [[CrossRef](#)]
59. Suhaimi, N.H.; Yeong, Y.F.; Ch'ng, C.W.M.; Jusoh, N. Tailoring CO₂/CH₄ Separation Performance of Mixed Matrix Membranes by Using ZIF-8 Particles Functionalized with Different Amine Groups. *Polymers* **2019**, *11*, 2042. [[CrossRef](#)] [[PubMed](#)]
60. Zakariya, S.; Yeong, Y.F.; Jusoh, N.; Tan, L.S. Performance of Multilayer Composite Hollow Membrane in Separation of CO₂ from CH₄ in Mixed Gas Conditions. *Polymers* **2022**, *14*, 1480. [[CrossRef](#)] [[PubMed](#)]
61. Zhu, X.; Yu, Z.; Wang, J.; Wang, P.; Li, X.; Long, R.; Wang, Q. Chemically stable NH₂-MIL-125(Ti)/Sep/PDA composite membranes with high-efficiency for oil/water emulsions separation. *Colloids Surf. A Physicochem. Eng. Asp.* **2022**, *646*, 128899. [[CrossRef](#)]
62. Pal, N.; Agarwal, M. Advances in materials process and separation mechanism of the membrane towards hydrogen separation. *Int. J. Hydrog. Energy* **2021**, *46*, 27062–27087. [[CrossRef](#)]
63. Li, G.; Kujawski, W.; Knozowska, K.; Kujawa, J. Thin Film Mixed Matrix Hollow Fiber Membrane Fabricated by Incorporation of Amine Functionalized Metal-Organic Framework for CO₂/N₂ Separation. *Materials* **2021**, *14*, 3366. [[CrossRef](#)]
64. Taurozzi, J.S.; Arul, H.; Bosak, V.Z.; Burban, A.F.; Voice, T.C.; Bruening, M.L.; Tarabara, V.V. Effect of filler incorporation route on the properties of polysulfone–silver nanocomposite membranes of different porosities. *J. Membr. Sci.* **2008**, *325*, 58–68. [[CrossRef](#)]
65. Ahmad, A.L.; Otitoju, T.A.; Ooi, B.S. Hollow fiber (HF) membrane fabrication: A review on the effects of solution spinning conditions on morphology and performance. *J. Ind. Eng. Chem.* **2019**, *70*, 35–50. [[CrossRef](#)]
66. Mubashir, M.; Yeong, Y.F.; Chew, T.L.; Lau, K.K. Optimization of spinning parameters on the fabrication of NH₂-MIL-53(Al)/cellulose acetate (CA) hollow fiber mixed matrix membrane for CO₂ separation. *Sep. Purif. Technol.* **2019**, *215*, 32–43. [[CrossRef](#)]
67. Ding, S.H.; Oh, P.C.; Mukhtar, H.; Jamil, A. Fabrication of NH₂-MIL-125 (Ti)/Polyvinylidene fluoride hollow fiber mixed matrix membranes for removal of environmentally hazardous CO₂ gas. *J. Nat. Gas Sci. Eng.* **2022**, *107*, 104794. [[CrossRef](#)]

Disclaimer/Publisher's Note: The statements, opinions and data contained in all publications are solely those of the individual author(s) and contributor(s) and not of MDPI and/or the editor(s). MDPI and/or the editor(s) disclaim responsibility for any injury to people or property resulting from any ideas, methods, instructions or products referred to in the content.